

Solid-State NMR Study of Different Types of Poly(vinyl formal)

P. Adriaenssens, I. Pollers, R. Carleer, D. Vanderzande, and J. Gelan*

*Limburg University, Instituut voor Materiaalonderzoek (IMO), Department SBG, Universitaire Campus, Gebouw D, B-3590 Diepenbeek, Belgium**Received August 3, 1998; Revised Manuscript Received November 6, 1998*

ABSTRACT: Several types of poly(vinyl formal) (PVF), copolymers of six-member formal rings and unreacted vinyl alcohol, prepared by different methods of synthesis out of atactic poly(vinyl alcohol) (PVA) were studied by NMR, thermal analysis, and wide-angle X-ray diffraction (WAXD). While thermal analysis and WAXD provide useful information about the macroscopic properties (e.g., T_g , crystallinity, T_m), solid-state NMR does focus more on the microscopic properties like molecular phase separation and molecular dynamics. The PVF polymers are composed of rigid and mobile molecular domains of which the distribution is mainly determined by the tacticity of the original atactic PVA polymer.

Introduction

As shown by the numerous studies described in the literature,^{1–4} solid-state NMR provides a way of investigating the motional characteristics of polymers. The NMR parameters T_1^H and $T_{1\rho}^H$, being the proton spin–lattice relaxation times in the lab and rotating frame, respectively, should however be interpreted with care due to the process of spin diffusion that is taking place very efficiently in rigid systems below the glass transition temperature, T_g . Below T_g they provide an excellent way to study molecular miscibility rather than mobility.²

In this paper, different types of poly(vinyl formal) (PVF) are studied by solid-state NMR techniques. PVF, a modification polymer of poly(vinyl alcohol) (PVA), is a copolymer of formal rings and unreacted vinyl alcohol. This complex polymer exhibits besides comonomer sequence microstructure also stereosequence (tacticity) microstructure. As described earlier,⁵ the distribution of functional groups (blocky or random) clearly depends on the modification method used. The percentage of reacted hydroxyl functions, expressed as the degree of acetalization, can easily be determined by liquid-state NMR.⁵

The nature of the relationship between the microscopic heterogeneity and the macroscopic properties of the system is related to the molecular motional characteristics of the different regions present in the sample. In general, the observed mechanical properties depend not only on the motional properties of these regions but also on their size, shape, and spatial distribution. In this paper, 1H and ^{13}C solid-state NMR measurements in combination with some macroscopic techniques as wide-angle X-ray diffraction (WAXD) and differential scanning calorimetry (DSC) are used to analyze the molecular structure and the mobility of the PVF samples in different time domains.

Experimental Section

Materials. Poly(vinyl formal) (PVF) is made from the condensation reaction of atactic poly(vinyl alcohol) (PVA) with formaldehyde. It is a copolymer of formal rings and unreacted vinyl alcohol. PVA, purchased from Aldrich, was purified by Soxhlet extraction with methanol. Molar mass and intrinsic viscosity were 123 000 g/mol and 0.998 dL/g, respectively. The tacticity of a-PVA was checked by 1H and ^{13}C liquid NMR. The triade fractions mm, mr, and rr were 0.22, 0.50, and 0.28,

Table 1. Water Content after Lyophilization until Constant Weight

| sample | degree of acetalization ^a (%) | water content ^b (% w/w) |
|-----------|--|------------------------------------|
| PVA | | 3.5 |
| PVF–HETa | 22 | 3.0 |
| PVF–HETb | 38 | 2.8 |
| PVF–HETc | 54 | 2.5 |
| PVF–HETd | 67 | 2.1 |
| PVF–PRECb | 35 | 2.9 |
| PVF–PRECc | 56 | 2.4 |
| PVF–PRECd | 63 | 2.2 |
| PVF–SOL | 98 | 1.8 |

^a Determined from liquid-state ^{13}C NMR spectroscopy. ^b Determined from quantitative 1H NMR spectroscopy in the liquid state.

respectively. The preparation of the different PVF samples is described elsewhere.⁵ The PVF samples labeled as PVF–HET (see Table 1) have a blocky distribution of functional groups, whereas samples noted as PVF–PREC exhibit random distribution. The PVF–SOL sample is prepared by the dissolution method and has a very high degree of acetalization. This degree of acetalization, reported in the second column of Table 1, represents the percentage of reacted hydroxyl functions during the modification reaction.⁵

NMR. All spectra were recorded on a Varian Inova spectrometer operating at a static magnetic field of 9.4 T. All polymer samples used were freeze-dried. The remaining water content was determined by 1H liquid NMR. Therefore, the samples were dissolved in dry perdeuterated dimethyl sulfoxide ($DMSO-d_6$) which provides the internal lock and chemical shift reference signal. The sample concentration was 3% (w/v). Quantitative spectra were recorded at 40 °C, using pulse widths of 10 μs (pulse angle 90°) and pulse intervals of 80 s. Spectra were obtained by accumulation of 8 scans. $DMSO-d_6$ was purchased from Merck (deuteration degree minimum 99.8%). Small amounts of water in $DMSO-d_6$ were removed by activated molecular sieves.

The 100 MHz solid-state CP/MAS ^{13}C NMR measurements were recorded at room temperature. Magic angle spinning was performed at approximately 6.5 kHz, making use of ceramic Si_3N_4 rotors. The Hartmann–Hahn condition ($\omega_{1H} = \gamma_H B_{1H} = \gamma_C B_{1C} = \omega_{1C}$) for cross-polarization was fixed using the aromatic signal of hexamethylbenzene. All T_1^H and $T_{1\rho}^H$ CP/MAS ^{13}C NMR experiments were run with a multipurpose pulse sequence⁶ in which a contact time for the CP process of 800 μs was used. The recycle time was 40 and 15 s for PVA and the different PVF samples, respectively. The spin lock field for the $T_{1\rho}^H$ measurements was 57 kHz.

The 400 MHz 1H solid-state wide-line measurements were performed at different temperatures with the solid echo⁷

method using an echo delay of 8 μ s. Alternation of the phase of the echo pulse while holding the phase of the read pulse constant was employed, in addition to the normal phase cycling, to minimize any residual effects due to receiver overload. Samples were measured in 5 mm Pyrex tubes fitted tightly with Teflon stoppers. To prevent annealing effects, a fresh sample was used for each T_2^H measurement of PVA above 130 °C.

Nonlinear least-squares multiexponential analyses of all relaxation data were accomplished on a Macintosh computer using the program KaleidaGraph 3.0.

DSC. The heat of fusion, the glass transition temperature (T_g), and/or the melting point (T_m) of the samples were obtained on a Perkin-Elmer 7, provided with a thermal analysis controller TAC/DX at a heating rate of 10 °C/min.

Wide-Angle X-ray Diffraction. Wide-angle X-ray diffraction patterns were obtained using a Philips PW1840 apparatus.

Results and Discussion

The PVF samples described differ in degree of acetalization, functional group distribution, degree of crystallinity, melting point (T_m), and/or glass transition temperature (T_g) (see further). These differences are closely related to each other. All samples are prepared, starting from atactic PVA. The sequence distribution of the functional groups in the resultant PVF polymers depends on the modification method used.⁵ In the "heterogeneous" method the reaction is carried out on water-swollen granular PVA. The formal rings are believed to be distributed selectively and collectively in the amorphous domains.^{8,9} This statement will be discussed later.

In the "precipitation" method the reaction initially takes place in an aqueous "solution" of PVA. At approximately 30% acetalization, the acetal precipitates after which the reaction continues heterogeneously. This method ensures a uniform distribution of functional groups.^{8,9}

In the "dissolution" method, the reaction is carried out on powdered PVA, suspended in dioxane, a good solvent for the acetal but a poor solvent for PVA. The reaction products (PVF) dissolve as the acetalization proceeds after which the reaction continues in the homogeneous system. The "dissolution" method is used to prepare PVA with a high degree of acetalization (PVF-SOL).

In the first part of the discussion an overview is given of a macroscopic investigation of the different PVF polymers. Subsequently, the amount of water after drying, the degree of crystallinity, and the glass transition temperature will be discussed.

The second part deals with the molecular dynamics of different PVF polymers by means of solid-state NMR.

Macroscopic Properties. Water Content. Since water has a softening effect on PVA and PVF polymers, it is important to know the amount of remaining water in these polymers in order to determine their physicochemical properties. Quantitative ^1H liquid NMR spectroscopy was used to determine the amount of water in the polymers after freeze-drying. Therefore, calibration samples of a fixed amount of dried DMSO- d_6 with a variable amount of added water were recorded. Linear least-squares fit of the water signal intensity vs the amount of added water (DMSO proton intensity fixed as internal reference) yields the concentration of water in the dried DMSO- d_6 . Polymer samples were dissolved in dried DMSO- d_6 , and quantitative ^1H liquid NMR spectra of these solutions (with known concentrations)

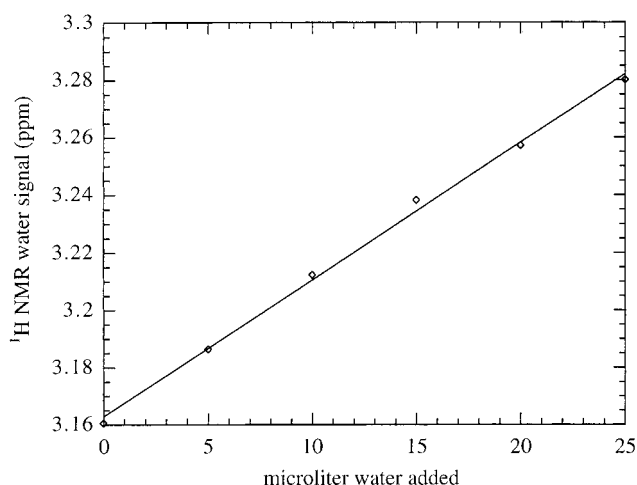


Figure 1. Linear relation between the chemical shift of the water resonance and the amount of water in DMSO- d_6 .

Table 2. Degree of Crystallinity, Melting Temperature, and Glass Transition Temperature as a Function of Degree of Acetalization

| sample | deg of acetalization ^a (%) | T_m^b (°C) | deg of crystallinity ^c (%) | T_g (°C) |
|-----------|---------------------------------------|--------------|---------------------------------------|------------|
| PVA | | 223 | 45 | 65 |
| PVF-HETa | 22 | 191 | 27 | 74 |
| PVF-HETb | 38 | 179 | 24 | 89 |
| PVF-HETc | 54 | 174 | 21 | 99 |
| PVF-HETd | 67 | 169 | 15 | 104 |
| PVF-PRECb | 35 | 160 | 8 | 71 |
| PVF-PRECc | 56 | 152 | 7 | 86 |
| PVF-PRECD | 63 | 152 | 5 | 91 |
| PVF-SOL | 98 | | | 107 |

^a Determined from liquid-state ^{13}C NMR spectra. ^b Determined from the peak maxima of the melting transition in the DSC thermogram. ^c Calculated from the surface under the melting peak using the heat of fusion of 100% crystalline PVA (159 J/g).

were recorded. The amount of water in the polymer samples can be found by subtracting the relative intensity of the water signal from the water intensity in the dried DMSO- d_6 . The remaining intensity yields the water concentration out of the calibration relation. The results are reported in Table 1. The amount of water varies between 2% and 3%. As a function of the degree of acetalization (with decreasing hydroxyl functions), a small decrease of the water content can be observed.

Hu et al.¹⁰ already mentioned that the chemical shift of the water signal in DMSO- d_6 depends on the concentration of the water. In Figure 1 the chemical shift of the water signal as a function of the amount of added water is shown. As can be seen, the relation between the chemical shift of the water signal in DMSO- d_6 and the concentration of water is linear. Therefore, the amount of water was also derived from the position of the water peak in the proton spectrum. The results obtained from signal area and chemical shift measurements are in good agreement with each other.

Degree of Crystallinity. PVA is a semicrystalline polymer, even in the atactic form.^{11–13} In the DSC thermogram the polymer exhibits a melting transition around 223 °C (Table 2). This melting peak is rather broad because of large differences in dimensions of the crystallites and different degrees of (im)perfection.¹⁴ The degree of crystallinity can be derived from the integration of the melting peak.

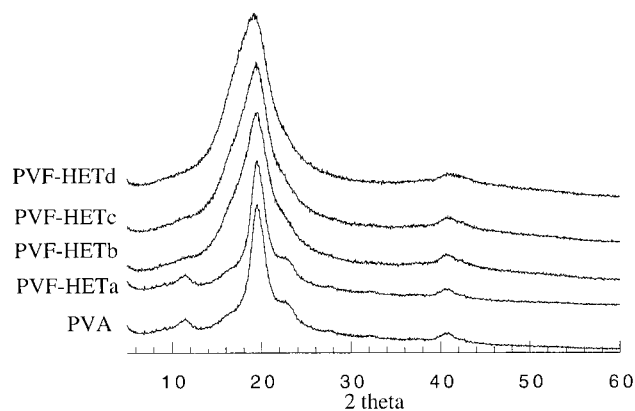


Figure 2. WAXD diffractograms of PVA and different PVF-HET polymers.

The degree of crystallinity of the PVF polymers is related to the modification method employed and to its degree of acetalization. Comparing the different modification methods mentioned above, it must be clear that in the "heterogeneous" samples the degree of crystallinity of PVA is less affected than in the "precipitation" and in the "dissolution" samples. The melting temperatures and the degrees of crystallinity of the different PVF polymers are reported in Table 2. For the calculation of the degree of crystallinity, the heat of fusion of 100% crystalline PVA (159 J/g)¹⁵⁻¹⁷ was used.

As can be seen in this table, the degree of crystallinity decreases with increasing degree of acetalization. The highest acetalized polymer, prepared by the dissolution method, is completely amorphous. Comparing the polymers prepared by the heterogeneous and the precipitation methods, one can notice that for a comparable degree of acetalization the polymers prepared by the heterogeneous method have a higher degree of crystallinity and a higher melting point. This difference can be explained as follows.

During the "precipitation" and "dissolution" modification methods, the crystallinity of PVA is fully destroyed since reaction takes places in solution. The unreacted hydroxyl units do not recrystallize (dissolution method) or only slightly (precipitation method) since the formal rings cannot be integrated in the crystal structure of PVA. In the PVF-HET samples, part of the crystallinity of the starting material (PVA) is not affected during the modification reaction, because the reaction takes place in the swollen state. The percentage crystallinity measured in these end products therefore represents "rest crystallinity" of PVA. In the heterogeneous reaction the amorphous regions become acetalized first. This explains why they can be described as block copolymers.⁵ As the acetalization increases, the crystalline regions react as well. Since the formal rings do not fit into the crystal lattice of PVA, the degree of crystallinity decreases. In the first step of the precipitation method, the crystallinity of PVA is destroyed by dissolving the polymer in hot water. During the acetalization process, the formal rings are built in randomly. The (unreacted) hydroxyl functions, which are distributed randomly as well, can only lead to a very limited degree of crystallinity.

This explanation is confirmed by wide-angle X-ray diffraction (WAXD) measurements (see Figures 2 and 3). The peak with $\theta = 19.5^\circ$ corresponds to the (110) reflection, i.e., a plane containing the planar zigzag chain direction of the crystallites.¹² The WAX diffrac-

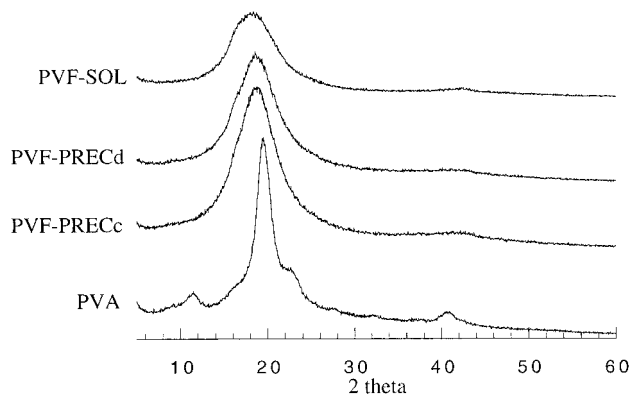


Figure 3. WAXD diffractograms of PVA, PVF-PRECC and d, and PVF-SOL.

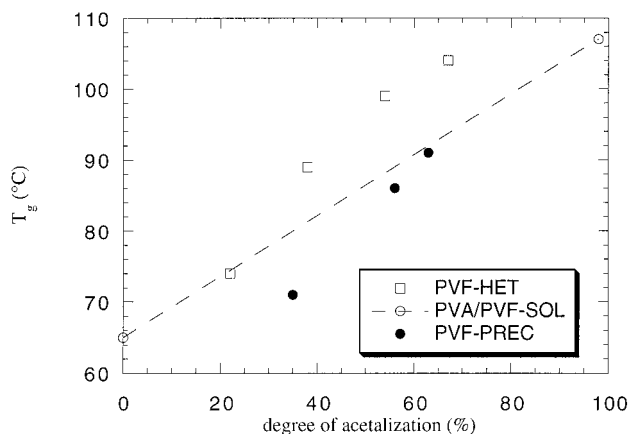


Figure 4. Glass transition temperatures of PVF-HET polymers and PVF-PREC polymers as a function of degree of acetalization. The values with a degree of acetalization of 0 and 98% refer respectively to PVA and PVF-SOL. History effects were destroyed in the first run by heating the samples until 40 °C above the glass transition temperature. The heating rate was 5 °C/min. The degree of acetalization was determined by liquid-state ¹³C NMR.⁵

togram of PVA-HETa and PVA are more or less identical. This may indicate that acetalization only has taken place in the amorphous domains. With increasing degree of acetalization, it becomes clear that the crystalline domains react as well, which results in a smaller amount of crystallinity (Table 2) and less perfect crystals.

Glass Transition Temperature (T_g). Water decreases the T_g of PVA and PVF polymers. The glass transition temperatures of PVA and the different types of PVF polymers (with a known amount of remaining water after drying) were determined by differential scanning calorimetry (DSC) and presented in Table 2. The measured T_g values of the polymers prepared by the heterogeneous and the precipitation method as a function of the degree of acetalization (copolymer composition) are shown in Figure 4. All T_g values are determined from the thermogram of the second run. A degree of acetalization equal to zero represents the T_g value of PVA while this with a degree of acetalization equal to 98% represents the T_g value of PVF-SOL.

Figure 4 shows that the glass transition temperature of PVF polymers increases with increasing degree of acetalization. At first sight, this phenomenon seems opposite to what is expected, because the introduction of formal rings causes a decrease of the number of (intra- and intermolecular) hydrogen bonds in the sample. In

PVA, the chain flexibility is mainly controlled by these inter- and intramolecular hydrogen bridges. With increasing temperature these bridges can be destroyed, resulting in a higher mobility of the polymer chain. The increase in T_g with increasing degree of acetalization can however be interpreted in terms of limited rotation around the backbone C–C bonds due to the formation of the six-member formal rings.

In Figure 4 one can see that the T_g of PVF–HET samples shows a clear positive deviation from the molar fraction weighted average T_g of the homopolymers. The opposite phenomenon is observed for PVF–PREC specimen. To explain this, one has to keep in mind that PVF–SOL (100% amorphous) has no crystallinity in contrast to PVF–HET samples while PVA is semicrystalline in contrast to PVF–PREC specimen which are almost fully amorphous. For PVF–HET samples, this positive deviation of T_g reflects strong intermolecular hydrogen bridge interactions arising from the “remaining crystalline PVA blocks” which cause an additional (in addition to acetalization) reduction of the mobility of the amorphous chains as compared to PVF–SOL. For PVF–PREC samples, being random copolymers with almost no crystallinity, the negative deviation of T_g can be explained by a relative increase in chain mobility (as compared to PVA) due to the absence of crystalline PVA blocks.

In general, the T_g –acetalization degree curves reflect a rather complex relation between degree of crystallinity, amount of formal rings, and amount and type of hydrogen bonds.

In summary, the DSC measurements show that acetalization leads to a nonlinear increase of the glass transition temperature of the amorphous phase. The introduction of formal rings reduces the conformational freedom of the polymer.

Microscopic Properties: Molecular Dynamics.

In the previous section the macroscopic properties of PVA and different PVF polymers were described. In the following section the molecular dynamics of this well-defined set of polymers will be discussed by means of ^{13}C and ^1H solid-state NMR techniques.

CP/MAS ^{13}C NMR. All, rather time-consuming, CP/MAS ^{13}C NMR (cross-polarization magic angle spinning) measurements were carried out at ambient temperature since PVA and PVF polymers decompose with increasing temperature as a function of time (yellow-brown coloring). The objective was to look for differences in molecular mobility and/or molecular organization between the different PVF polymers.

Figure 5 shows the CP/MAS ^{13}C NMR spectrum of dry atactic PVA and dry PVF samples prepared by different modification methods. All resonances in the range 30–50 ppm arise from methylene C_4 carbons, those between 55 and 83 ppm from methine C_1 and C_3 carbons, and those between 83 and 100 ppm from methylene C_2 carbons. The region 83–100 ppm consists of C_2 carbons in meso rings (90–100 ppm) and racemic rings (83–90 ppm).

Analysis of T_1^H and $T_{1\rho}^H$ Relaxation Times. The presence of multiple environments having different molecular dynamics can be studied using several relaxation time constants. For the interpretation of these relaxation times, it is important to realize that ambient temperature is situated below the glass transition

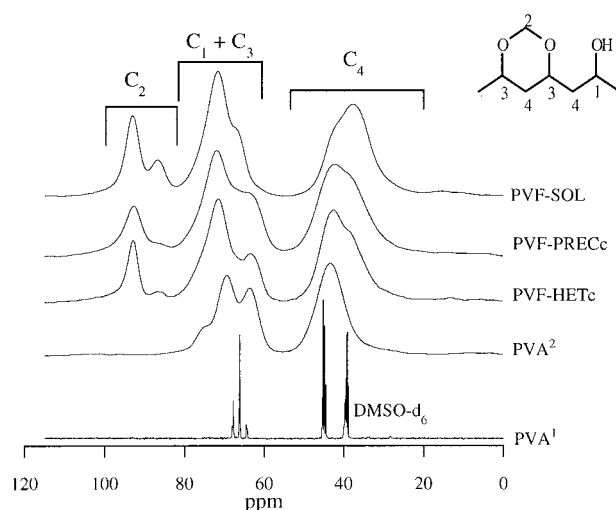


Figure 5. The 100 MHz ^{13}C CP/MAS spectra of PVA², PVF–HETc, PVF–PRECC, and PVF–SOL at ambient temperature. PVA¹: 100 MHz liquid ^{13}C NMR spectrum of a 7.5% solution of PVA in DMSO- d_6 at 80 °C.

temperature of PVA and all PVF polymers. So, for T_1^H (spin–lattice) and $T_{1\rho}^H$ (spin–lattice in rotating frame) the process of spin diffusion is taking place rather efficiently.

In a multiphase system below T_g , T_1^H and $T_{1\rho}^H$ provide information about the molecular morphology involved in the spin system due to spin diffusion. Proton $T_{1\rho}$ values will be averaged out over a short distance (on the order of 1 nm) by spin diffusion, making it a rather local property. Since $T_{1\rho}^H$ relaxation times are sensitive to frequencies of several tens of kilohertz, they reflect the motion of short segments in the polymer chain. T_1^H is sensitive to the Larmor frequency range (several 100 MHz) and is averaged out over a larger distance (on the order of tens of nanometers), making it a more large-scale molecular property. The maximum diffusive path length L , over which proton–proton spin diffusion can occur, can be approximated by $L = (6DT_1)^{1/2}$, where D is the spin diffusion coefficient ($\approx 10^{-16} \text{ m}^2/\text{s}$ for rigid solids) and T_1 being T_1^H or $T_{1\rho}^H$.¹⁸ Multiple relaxation times will be observed only if the domain sizes are larger than L and if the intrinsic relaxation times (molecular dynamics) of the domains are sufficiently different. So, $T_{1\rho}^H$ and T_1^H offer an interesting possibility to estimate the minimum and maximum dimensions of the molecular domains.

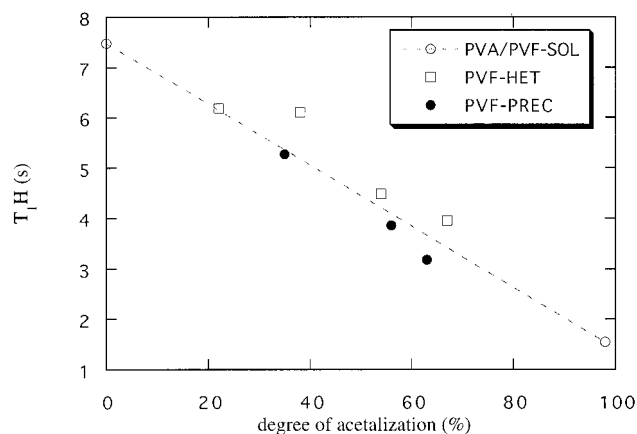
T_1^H values, measured via ^{13}C magnetization by the inversion recovery CP/MAS method, were analyzed first since they are needed to determine the preparation delay ($5T_1^H$) for all later CP/MAS experiments. For all species T_1^H values can be fitted monoexponentially and are, within each sample, similar for all carbon resonances due to spin diffusion. Moreover, they are in agreement with those determined directly by ^1H wide-line experiments (see Table 3). This means that if a two-phase structure is present, the T_1^H values of both phases will be averaged out due to spin diffusion. Furthermore, one has to be careful not to compare different species (e.g., HETc and PRECC) only in terms of molecular mobility since T_1^H also depends on the average internuclear proton distance ($\sim 1/r^6$) which can be quite different.

As for T_g , T_1^H will, due to spin diffusion, reflect the molar fraction weighted average of the T_1^H values of the homopolymers. Figure 6 shows the relation between T_1^H

Table 3. T_1^H Values at Ambient Temperature and 100 °C Determined by Proton Wide-Line NMR^a

| sample | T_1^H (s) at ambient temp | T_1^H (s) at 100 °C |
|-----------|-----------------------------|-----------------------|
| PVA | 7.48 (0.04) | 1.66 (0.02) |
| PVF-HETa | 6.18 (0.08) | 1.54 (0.04) |
| PVF-HETb | 6.11 (0.09) | 1.92 (0.02) |
| PVF-HETc | 4.48 (0.06) | 2.87 (0.03) |
| PVF-HETd | 3.95 (0.05) | 3.75 (0.03) |
| PVF-PRECb | 5.27 (0.04) | 1.64 (0.04) |
| PVF-PRECC | 3.86 (0.06) | 1.76 (0.01) |
| PVF-PRECD | 3.18 (0.07) | 2.83 (0.03) |
| PVF-SOL | 1.55 (0.02) | 2.67 (0.03) |

^a The 95% confidence limits are between parentheses.

**Figure 6.** Relation between T_1^H (at ambient temperature) and the degree of acetalization of different PVF-HET and PVF-PREC samples. The values with a degree of acetalization of 0 and 98% refer respectively to PVA and PVF-SOL.

and the degree of acetalization. In general, T_1^H indeed reflects the molar composition of the copolymers. In agreement with the relation between T_g and the degree of acetalization, the T_1^H values of PVF-HET samples tend to show a positive deviation from the molar fraction weighted average while the PVF-PREC samples rather show the opposite phenomenon. As for the T_g -acetalization relation, this can be explained by the remaining crystalline PVA blocks in the PVF-HET specimen (in contrast to amorphous PVF-SOL) and by the lack of almost all crystallinity in PVF-PREC samples (in contrast to semicrystalline PVA).

Increasing the temperature to 100 °C increases molecular dynamics since intermolecular H-bonds partly will be broken and the temperature becomes closer to (or exceeds) T_g . Table 3 clearly shows that the relative change of T_1^H in going from ambient temperature to 100 °C decreases as a function of the degree of acetalization or, in other words, as a function of T_g increase. For HETa, e.g., having a $T_g = 74$ °C, a decrease for T_1^H of about 4.6 s is observed while for HETd, having a T_g of 104 °C, one can hardly notice any increase in density of molecular motions on the time scale detected by T_1^H relaxation. This is in agreement with T_1 minima of polymers that normally appear at temperatures above $T_g + 30$ –50 °C. All PVF-HET, PVF-PREC, and PVA species are at ambient temperature situated at the right side of the minimum in the $\log T_1^H$ – $\log \tau_c$ correlation diagram (τ_c is the correlation time of molecular motion). Only amorphous PVF-SOL, having the highest T_g of 107 °C, has an increasing T_1^H value as a function of temperature. A more detailed study as a function of temperature is however needed if one wants to explain this in more detail.

$T_{1\rho}^H$ was measured using the delayed cross-polarization method described by Aufla et al.¹⁹ in which the proton magnetization after the initial 90° pulse is kept in spin lock for a variable evolution time t . After this variable spin lock time the magnetization is cross-polarized to the carbon nuclei during a fixed contact time CT. Detection occurs under high power proton decoupling. $T_{1\rho}^H$ of each phase can be determined using the following adapted equation:

$$M(t) = \sum M_{oi} \exp[-(CT + t)/T_{1\rho}^H i]$$

in which $M(t)$ is the overall magnetization as a function of the variable evolution time t . The evolution time is extended with the contact time CT, during which $T_{1\rho}^H$ relaxation further occurs. Table 4 shows the results for PVA, PVF-HETc, PVF-PRECC, and PVF-SOL.

Similar results (not shown) were obtained by the classical cross-polarization experiment in which the proton magnetization after the 90° pulse is transferred to carbon during a variable contact time under spin lock conditions.

For all species, the relaxation data have to be analyzed biexponentially. Notice that one is looking now to much smaller molecular regions (on the order of 1 nm), in contrast to T_1^H where one looks on the average to the global copolymer composition (order of 10 nm). The following relation was used for the nonlinear least-squares fit (Marquardt–Levenberg algorithm):

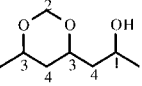
$$M(t) = M_{o1} \exp[-(CT + t)/T_{1\rho}^H 1] + M_{o2} \exp[-(CT + t)/T_{1\rho}^H 2]$$

Changing the spin lock field strength from 57 to 40 kHz resulted in a decrease of both $T_{1\rho}^H$ values from 1.7 and 5.8 ms to 0.7 and 2.4 ms for PVF-HETc with conservation of the fractional distribution. A decrease of $T_{1\rho}^H$ values was also observed upon adding water. This can easily be explained by the plastifying effect (increase of molecular mobility) of water on PVF polymers. Both observations allow to conclude that the correlation times of molecular motion are situated at the right side of the minimum in the $\log T_{1\rho}^H$ – $\log \tau_c$ correlation diagram. So as expected, the longest $T_{1\rho}^H$ component can be ascribed to the rigid fraction while the short $T_{1\rho}^H$ component corresponds to the mobile fraction.

All $T_{1\rho}^H$ values are, within their region, similar for all carbon resonances due to efficient local spin diffusion. Based on the $T_{1\rho}^H$ values (Table 4), the minimum size has to be larger than about 1 and 2 nm for the mobile and rigid regions, respectively. Again, one has to be careful not to compare different species (e.g., HETc and PRECC) only in terms of molecular mobility since $T_{1\rho}^H$ also depends on the average internuclear proton distance ($\sim 1/r^6$) which can be quite different.

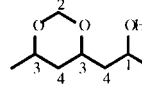
Remarkable is the fact that for all samples, independent of the degree of acetalization, the functional group distribution, the degree of crystallinity, etc., the fractional distribution is rather similar (65–70/35–30). Since similar fractions are observed even for PVF-SOL (fully amorphous), the rigid fraction cannot simply be assigned to the crystalline phase, although if crystallinity is present, it certainly will be part of it. This is confirmed by the C₂ signal (specific for acetal rings) which also shows the same behavior while crystallinity mainly occurs in nonacetalized domains. The biexponential behavior cannot be fully explained by the

Table 4. Overview of $T_{1\rho}^H$ Values with 95% Confidence Limits between Parentheses^a

|  | signal | $T_{1\rho}^H(1)$ (ms) | M_{01} % | $T_{1\rho}^H(2)$ (ms) | M_{02} % |
|---|---------------------------------|--------------------------|---------------|--------------------------|---------------|
| PVA | C ₁ | 1.5 (0.3) | 34 (3) | 5.4 (0.3) | 66 (5) |
| | C ₄ | 1.5 (0.2) | 32 (2) | 5.5 (0.2) | 68 (3) |
| | sum | 1.5 (0.2) | 33 (2) | 5.5 (0.2) | 67 (3) |
| | | | | | |
| PVF-HETc | C ₂ | 1.4 (0.6) | 25 (5) | 5.0 (0.3) | 75 (7) |
| | C ₁ + C ₃ | 1.7 (0.2) | 30 (2) | 5.9 (0.2) | 70 (3) |
| | C ₄ | 1.9 (0.4) | 29 (5) | 6.0 (0.3) | 71 (6) |
| | sum | 1.7 (0.3) | 28 (3) | 5.8 (0.2) | 72 (4) |
| PVF-PRECC | C ₂ | 1.9 (0.4) | 32 (9) | 4.7 (0.4) | 63 (9) |
| | C ₁ + C ₃ | 2.0 (0.5) | 38 (9) | 4.7 (0.5) | 62 (10) |
| | C ₄ | 1.7 (0.3) | 37 (8) | 4.8 (0.3) | 63 (9) |
| | sum | 1.5 (0.3) | 34 (5) | 4.7 (0.3) | 66 (7) |
| PVF-SOL | C ₂ | 2.8 (1.0) | 34 (3) | 7.4 (1.1) | 66 (5) |
| | C ₁ + C ₃ | 2.5 (0.8) | 33 (2) | 7.2 (0.8) | 67 (4) |
| | C ₄ | 3.2 (1.2) | 37 (6) | 7.5 (1.5) | 63 (7) |
| | sum | 2.7 (0.8) | 33 (2) | 7.3 (0.9) | 67 (3) |

^a The contact time was 800 μ s, and the spin-lock time was varied between 0.1 and 15 ms. The repetition time for the PVF polymers and for PVA was 15 and 40 s, respectively.

Table 5. T_1^C Values Measured with the Torchia Pulse Sequence^a

|  | signal | $T_1^C(1)$ (s) | M_{01} % | $T_1^C(2)$ (s) | M_{02} % |
|--|---------------------------------|-------------------|---------------|-------------------|---------------|
| PVF-HETc | C ₁ + C ₃ | 9.3 (0.9) | 36 (2) | 65.4 (3.2) | 64 (3) |
| | C ₄ | 8.2 (0.8) | 38 (2) | 65.0 (3.3) | 62 (2) |
| | sum | 8.7 (0.7) | 36 (2) | 65.5 (3.3) | 64 (2) |
| | | | | | |
| PVF-PRECC | C ₁ + C ₃ | 4.7 (1.0) | 35 (3) | 48.3 (3.2) | 65 (4) |
| | C ₄ | 4.4 (1.1) | 39 (5) | 49.3 (5.4) | 61 (5) |
| | sum | 6.0 (1.5) | 30 (4) | 47.8 (3.9) | 70 (5) |
| | | | | | |

^a The contact time was 800 μ s, and the repetition time was 15 s. The evolution time was varied between 0.005 and 100 s. The 95% confidence limits are between parentheses.

acetalization, where the formal rings would be responsible for the rigid component, since also PVA, having no formal rings, shows the same biexponential behavior.

Hydrogen bridges could also be responsible for a difference in molecular mobility. One could imagine local spots in the amorphous phase of the polymer where the probability of appearance of intermolecular hydrogen bonds is higher. These regions would have a more rigid character. For the semicrystalline samples, crystallinity will be part of this rigid component.

Analysis of T_1^C Relaxation Times. Another relaxation time constant that is often used to study semicrystalline species is T_1^C .²⁰ Due to the low natural abundance of ¹³C spins, spin diffusion is rather inefficient for the carbon nuclei. The T_1^C relaxation time therefore can be interpreted more in terms of local molecular dynamics. Due to faster molecular motion in the amorphous regions, T_1^C of the amorphous component normally is much shorter than T_1^C of the crystalline component.

The T_1^C measurements were accomplished with the Torchia sequence,²¹ and the results fitted to the follow-

ing equation:

$$M(t) = \sum 2M_{0i} \exp(-t/T_{1i}^C)$$

Table 5 shows the results for PVF-HETc and PVF-PRECC having almost the same degree of acetalization, thus comonomer content. Although PRECC is almost completely amorphous, a biexponential fitting had to be used for both samples, yielding again the same fractional distribution (65–70/35–30). Although Hu et al.²² (single crystals) and Hori et al.²³ analyze the T_1^C results of PVA, obtained by the same pulse sequence, in terms of three components, such analysis was not possible on our T_1^C data of the PVF specimen (two time constants of three always converged toward the same value). So as for the $T_{1\rho}^H$ results, the fractional ratio cannot be explained solely by crystallinity.

Hu et al.²² showed by Torchia T_1^C measurements on PVA that the amount of intramolecular H-bonds is higher for the noncrystalline regions (fast relaxing component) while the crystalline regions (slow relaxing

component; $T_1^C \sim 65$ s according to Hori et al.²³) have more intermolecular H-bonds, causing an increased rigidity.

Having this information, the results can be explained as follows: in the synthesis of HETc, part of the PVA crystallinity is preserved, giving rise to strong intermolecular H-bonds between hydroxyl functional groups. Additionally, regions rich in intermolecular H-bonds between hydroxyl groups and formal rings will contribute to the rigid fraction. Neither T_1^C nor $T_{1\rho}^H$ relaxation data are able to differentiate between these contributions. For PRECc, all PVA crystallinity is destroyed during acetalization in solution, and the formal rings are built in randomly. Intermolecular H-bonds between hydroxyl group sequences will now give rise only to the small crystalline fraction. Intermolecular H-bonds between hydroxyl groups and formal rings will not result in crystallinity but will cause a decrease of local molecular mobility. The difference in T_1^C between HETc and PRECc can, besides to the remaining crystallinity in HETc, also be caused by differences in local proton environment.

Since the probability of a hydroxyl functional group in PVA to form an intra- or intermolecular hydrogen bond is highly determined by the tacticity of the polymer (atactic PVA is used in this study), it seems normal that the fractions of the mobile and rigid components in HETc and PRECc are rather similar.

In general, it can be concluded that the tacticity of the starting PVA polymer, ruling the amount of intermolecular H-bonds, determines the fractional distribution of the mobile and rigid components observed by the local NMR parameters $T_{1\rho}^H$ and T_1^C in these PVA-derived polymers. The time constants of both components are difficult to interpret since they represent besides differences in molecular mobility also possible differences in average proton environment. This is in contrast to T_1^H , which due to spin diffusion is a more large-scale molecular property. It enables to observe the overall mobility-reducing effect of the remaining crystalline PVA blocks on the amorphous phase of the PVF-HET specimen.

¹H Solid-State Wide-Line NMR. Although ¹H wide-line spectra of polymers do not provide chemical shift information, they are very sensitive toward the detection of multiphase behavior (especially T_2^H) and molecular miscibility (especially T_1^H due to spin diffusion).

The advantage is that they can be acquired rather fast (only a few minutes for a T_2^H measurement). T_1^H values for the different polymers are shown in Table 3 and are already discussed in the previous CP/MAS ¹³C NMR section.

T_2^H measurements at ambient temperature show that below the glass transition, as expected,²⁴ no differences in molecular mobility are observed. The relaxation decay is monoexponential and could be fitted by a single Gaussian function. The fit resulted in a similar value of ± 10 μ s for PVA and all PVF polymers. This means that the relaxation is dominated by static contributions which are for both crystalline and amorphous glass regions excessively present.

At temperatures above T_g , the difference in mobility between crystalline and amorphous regions increases considerably especially since intermolecular hydrogen bonds in amorphous regions will be broken.

Table 6 shows the T_2^H of PVF-SOL as a function of temperature, starting from 90 °C. Below 90 °C the FID

Table 6. T_2^H Values of PVF-SOL in the Temperature Interval 90–150 °C^a

| temp (°C) | T_2^H (μ s) | temp (°C) | T_2^H (μ s) |
|-----------|--------------------|-----------|--------------------|
| 90 | 11.9 (0.1) | 130 | 22.4 (0.2) |
| 100 | 12.7 (0.1) | 140 | 38.9 (0.2) |
| 110 | transition | 150 | 65.2 (0.2) |
| 120 | transition | | |

^a The 95% confidence limits are between parentheses.

Table 7. T_2^H Values of PVA in the Temperature Interval 50–170 °C^a

| temp (°C) | $T_2^{H(1)}$ (μ s) | M_{01} (%) | $T_2^{H(2)}$ (μ s) | M_{02} (%) |
|-----------|-------------------------|--------------|-------------------------|--------------|
| 50 | 10.0 (0.1) | | | |
| 60 | 10.3 (0.1) | | | |
| 70 | 10.7 (0.1) | | | |
| 80 | 11.3 (0.1) | | | |
| 90 | 11.8 (0.1) | 97 (1) | 35 (7) | 3 (1) |
| 100 | 12.2 (0.1) | 93 (2) | 34 (2) | 7 (1) |
| 110 | 12.4 (0.1) | 86 (1) | 33 (1) | 14 (2) |
| 120 | 12.5 (0.1) | 81 (2) | 33 (1) | 19 (2) |
| 130 | 12.6 (0.1) | 77 (1) | 35.7 (0.8) | 23 (1) |
| 140 | 12.7 (0.1) | 74 (1) | 46.7 (0.8) | 26 (2) |
| 150 | 12.6 (0.1) | 70 (2) | 43.8 (0.6) | 30 (1) |
| 160 | 12.7 (0.1) | 57 (1) | 140 (1) | 43 (1) |
| 170 | 12.1 (0.1) | 49 (2) | 145.2 (0.4) | 51 (2) |

^a The 95% confidence limits are between parentheses.

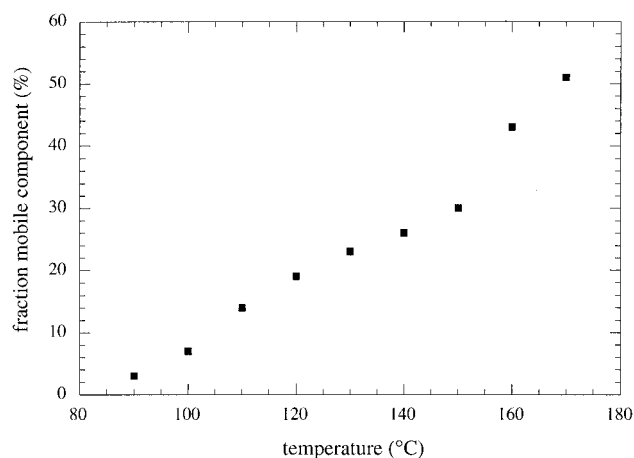


Figure 7. Overview of the fraction of the mobile component in PVA in the temperature interval 90–170 °C.

can be analyzed by a single Gaussian function with a $T_2^H \sim 12$ μ s. Between 90 and 120 °C (around the glass transition) the analysis of the FID is rather complicated. Neither a single Gaussian function nor a biexponential analysis with a Gaussian and exponential function yields an optimal fit. Around the secondary T_g transition a broad distribution of correlation times is present in the system. From 130 °C on, the FID can be analyzed by a single-exponential function (Lorentzian line shape), and the value of T_2^H increases rather fast as a function of temperature.

Table 7 shows T_2^H of PVA as a function of temperature. Up to 80 °C the T_2^H decay is monoexponential (Gaussian function) with a $T_2^H \sim 10$ μ s. With increasing temperature the T_2^H relaxation shows a biexponential decay that can be fitted to a Gaussian and exponential function. As expected, a decrease of the rigid fraction toward a value representative for the amount of crystallinity is observed. Figure 7 shows the fraction of mobile component as a function of temperature. Up to 150 °C, the fraction of the mobile component increases almost linearly. Above 150 °C (± 85 °C above T_g) a much faster increase of the mobile fraction and its T_2^H relaxation

time constant is observed. Although the T_2^H measuring time is rather short (a few minutes), a fresh sample was used for each measurement at temperatures above 130 °C to prevent annealing. Complete line shape separation between the crystalline and amorphous fraction is only obtained at temperatures around $T_g + 50\text{--}100$ °C.²⁴

Conclusions

High-resolution CP/MAS ^{13}C NMR measurements show that semicrystalline as well as amorphous PVF polymers consist of a mobile and rigid component. This difference in molecular mobility cannot solely be explained in terms of amorphous and crystalline character of the components, but results from the distribution of intra- and intermolecular hydrogen bonds that is determined by the intrinsic tacticity of the original PVA. The crystalline component of the semicrystalline PVF specimen forms part of the rigid component of which the amount of intermolecular hydrogen bonds is larger than for the mobile component.

Besides information about the dimensions of molecular regions (T_1^H and $T_{1\rho}^H$), T_1^H , $T_{1\rho}^H$, and T_1^C provide useful insight into the molecular dynamics of the polymers.

Proton T_2^H wide-line measurements as a function of temperature show that the difference in molecular mobility between crystalline and amorphous domains only increases considerably far above the glass transition. The T_2^H relaxation of PVA shows a biexponential behavior. The fraction of the rigid component decreases and approximates the amount of crystallinity present in the specimen at temperatures about 100 °C above T_g .

Acknowledgment. This research is performed as part of the program "InterUniversity Attraction Pole" (IUAP; Contract P4/11) supported by the Belgian Gov-

ernment Services of the Prime Minister—Federal Services for Scientific, Technical and Cultural Affairs.

References and Notes

- (1) Komoroski, R. A. *High-Resolution NMR Spectroscopy of Synthetic Polymers in Bulk*; VCH: New York, 1986.
- (2) Fyfe, C. A. *Solid State NMR for Chemists*; C. F. C. Press: Ontario, Canada, 1984.
- (3) Ibbett, R. N. *NMR Spectroscopy of Polymers*; Chapman & Hall: London, 1993.
- (4) Friebolin, H. *Ein- und zweidimensionale NMR-Spektroskopie*; VCH: Weinheim, 1991.
- (5) Pollers, I.; Adriaensens, P.; Carleer, R.; Vanderzande, D.; Gelan, J. *Macromolecules* **1996**, *29*, 5875.
- (6) Hoogmartens, I.; Adriaensens, P.; Vanderzande, D.; Gelan, J. *Anal. Chim. Acta* **1993**, *283*, 1025.
- (7) Powles, J. G.; Strange, J. H. *Proc. Phys. Soc.* **1963**, *82*, 6.
- (8) Toyoshima, K. *Polyvinyl Alcohol—Properties and Applications*; John Wiley & Sons: Chichester, 1973; p 394.
- (9) Sakurada, I.; Fuchino, K. *Riken Iho* **1941**, *20*, 298.
- (10) Hu, S.; Horii, F.; Odani, H. *Bull. Inst. Chem. Res., Kyoto University* **1989**, *67* (5–6), 239.
- (11) Bunn, C. W. *Nature* **1948**, *161*, 929.
- (12) Mooney, R. C. L. *J. Am. Chem. Soc.* **1941**, *63*, 2828.
- (13) Finch, C. A. *Polyvinyl Alcohol—Developments*; John Wiley: Chichester, 1992.
- (14) Richardson, M. J. In *Developments in Polymer Characterization*; Dawkins: London, 1978.
- (15) Brandrup, J.; Immergut, E. H. *Polymer Handbook*, 3rd ed.; John Wiley & Sons: New York, 1989.
- (16) Tsuboi, K.; Mochizuki, T. *J. Polym. Sci., Part B* **1963**, *1*, 531.
- (17) Wunderlich, B. *Macromolecular Physics*; Academic Press: New York, 1980.
- (18) Douglas, D. C.; Jones, G. P. *J. Chem. Phys.* **1966**, *45*, 956.
- (19) Aufla, R. S.; Harris, R. K.; Packer, K. J.; Parameswaran, M.; Say, B. J.; Bunn, A.; Cudby, M. E. A. *Polym. Bull.* **1982**, *8*, 253.
- (20) Hirai, A.; Horii, F.; Kitamaru, R.; Fatou, J. G.; Bello, A. *Macromolecules* **1990**, *23*, 2913–291.
- (21) Torchia, D. J. *Magn. Reson.* **1978**, *30*, 613.
- (22) Hu, S.; Tsuji, M.; Horii, F. *Polymer* **1994**, *35*, 2516.
- (23) Horii, F.; Hu, S.; Ito, T.; Odani, H.; Kitamaru, R.; Matsuzawa, S.; Yamaura, K. *Polymer* **1992**, *33*, 2299.
- (24) Fedotov, V. D.; Schneider, H. *Structure and Dynamics of Bulk Polymers by NMR-Methods*; Springer-Verlag: Berlin, 1989.

MA981216C